ACS APPLIED MATERIALS & INTERFACES

Research Article

www.acsami.org

Polymeric Nanocylinders by Combining Block Copolymer Self-Assembly and Nanoskiving

Mohammadreza Nasiri,[†] Arthur Bertrand,[†] Theresa M. Reineke,* and Marc A. Hillmyer*

Department of Chemistry, University of Minnesota, Minneapolis, Minnesota 55455-0431, United States

Supporting Information

ABSTRACT: A new facile fabrication approach to generate polymeric nanostructures is described. Block copolymers containing immiscible segments can self-assemble to generate ordered nanostructures, such as cylinders of one block in a matrix of the other in the bulk, which can then be sectioned on the nanoscale using a microtome (nanoskiving). Dispersing these sections in a selective solvent for the matrix block results in nanocylinders. In one example, we utilized a poly(*N*,*N*-dimethylacrylamide)-*block*-poly(styrene) (PDMA−PS) copolymer containing 36% by volume of PS. This composition was selected as it self-assembles into cylinders of PS in a matrix of PDMA. Following a previously described procedure, the cylinders were aligned using a channel die. The aligned samples were subsequently sectioned using a microtome containing a diamond knife and dispersed in water, a selective solvent for the PDMA matrix, affording PS nanocylinders with a PDMA corona. This technique allows tuning of nanocylinders without the requirement of specialty fabrication equipment.

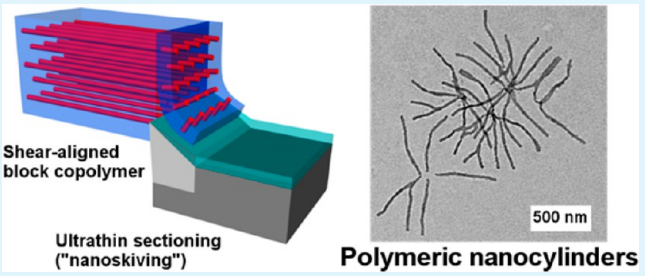

KEYWORDS: *polymeric nanoparticles, nanoskiving, block copolymer self-assembly, nanocylinders*

INTRODUCTION

Polymeric nanoparticles are utilized in different research disciplines, including delivery vehicles in the field of nanomedicine.[1] To fine-tune nanosystems for various applications, new methods are needed to fabricate particles with tunable sizes, specific shapes, and homogeneous surfaces. Nanoparticle fabrication methods are generally divided into "top−down" and "bottom−up" approaches. In top down methods, the desired dimensions are typically achieved by reducing the size of an object with larger dimensions in a mechanically controlled manner. Conversely, a bottom-up approach typically corresponds to self-assembly of molecular constituents into supramolecular nanoscale assemblies.[2]

In general, bottom-up nanoparticle fabrication methods, based on precipitation methods, yield spherical nanoparticles of various sizes with narrow size distributions.[3] Also, there are examples in the literature where cylindrical micelles are generated using dissolution techniques.[4−6] However, size control can be difficult to achieve and maintain because of molecular rearrangement and potential morphological transitions, although molecular exchange can be a very slow process as revealed by small-angle scattering experiments.[7,8] On the other hand, lithographic and imprinting methods are able to produce nanoparticles with controlled sizes and various shapes via top-down approaches. For example, in the photolithographic process, particles can be formed by irradiating a film of photoresist with UV light through a mask of the desired shape. The nanoparticles can then be harvested by washing off the unexposed material along with the sacrificial layer underneath.[9] Although this technique has an excellent control over the size and shape of the particles, a UV-curable material is required, thus dramatically restricting the range of particles achievable.[10] To resolve this issue, imprinting techniques have been developed where only the initial master template needs to be formed via lithography, such as soft lithography, and then particle replication in nonwetting templates (PRINT) technology is used to form the nanoobjects of various sizes and shapes.[1]

With the ability to fabricate nearly monodisperse particles in the range of 10 nm−200 μm,[10] high precision and versatility on the shape of particles and scalability, PRINT technology is a leading method for nanoparticle fabrication. In the PRINT process, a patterned fluorocarbon-based mold is filled with the materials of interest followed by lamination with a high-surface-energy material. Peeling off the laminate material removes all the excess solution from the mold. After the curing and solidification steps, an adhesive layer is used to harvest the cured particles. Dissolution of the adhesive layer results in a solution containing free particles.[11] PRINT employs several steps with particular requirements and access to the requisite fabrication equipment. While PRINT represents an elegant and successful strategy, a potential limitation for this and related top-down nanoparticle fabrication methods, is the generation of particles with imperfect surfaces.[3] On the other hand, generally, in a bottom-up approach, particles are formed in their thermodynamically stable state, typically resulting in homogeneous surfaces with minimum defects.[12]

Received: July 9, 2014
Accepted: August 25, 2014
Published: September 3, 2014

Because of their ability to self-organize into predictable nanostructures, block copolymers can adopt structures with controlled dimensions and high aspect ratios desirable for the fabrication of nanostructured materials.[13] In particular, several studies demonstrated the possibility to macroscopically orientate the microstructure of self-assembled block copolymers.[14−17] With these properties of bulk block copolymers in mind, we were inspired by the work of Whitesides and co-workers, who developed a new technique for nanostructure fabrications called "nanoskiving", combining deposition of metals on a substrate and thin sectioning with an ultramicrotome process.[18−20] They showed the applicability of this technique for simple structures such as nanowires, as well as more complex nanostructures.

Herein, a novel top-down particle fabrication approach combining bottom-up block copolymer self-assembly and nanoskiving is investigated. Monolithic specimens were generated from diblock copolymers with a composition tuned to self-assemble into a cylindrical morphology, followed by microstructural alignment using a channel die. Afterward, the specimen was cut to thin slices with defined thicknesses using a microtome equipped with a diamond knife. Finally, dispersion of the cut slices into a selective solvent for the matrix block resulted in nanocylinders of the minor component with coronae of the major component (Figure 1). Unlike cylindrical micelles, our

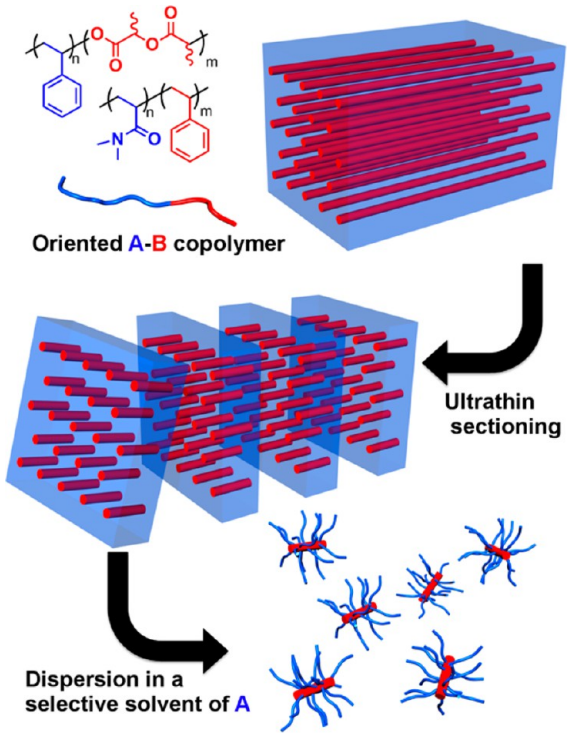

Figure 1. Schematic representation of nanoparticle generation combining block copolymer self-assembly and nanoskiving.

BCP-based strategy relies on bulk self-assembly and mechanical down-sizing, thus providing shape stability and some degree of length control of the nanocylinders.

RESULTS AND DISCUSSION

To explore the idea of nanoparticle fabrication via nanoskiving of bulk ordered block copolymer structures, a polystyrene-*b*-polylactide (PS-*b*-PLA) copolymer was synthesized according to a previously reported procedure by a combination of anionic and ring opening transesterification polymerization (ROTEP) techniques.[14] The molar masses for the PS and PLA blocks were determined to be 42 kg/mol and 18 kg/mol, respectively, by ^{1}H NMR spectroscopy (see Figure S1 in the Supporting Information for polymer characterization details). Based on the calculated PLA volume fraction (0.26), a microstructure composed of PLA cylinders in a PS matrix is expected.[14] The copolymer was processed in a home-built channel die at 130 °C to produce microstructurally aligned PS−PLA monoliths (Figure 3a).[15] Microstructure characterization was performed via small-angle X-ray scattering (SAXS) analysis of the oriented PS−PLA monolith at 25 °C and revealed an intense primary peak at $q^* = 0.165$ nm^{-1} ($D^* = 38.1$ nm), along with a prominent peak at $\sqrt{7}q^*$, consistent with a cylindrical morphology (Figure 2).

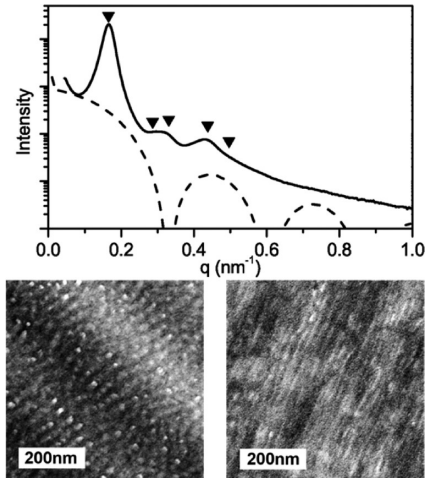

Figure 2. (Solid line) Experimental 1D synchrotron SAXS profile of shear-oriented PS−PLA monolith at 25 °C and (dashed line) simulated form factor scattering curve generated for cylinders with a 11.8 nm radius (value extracted from the experimental SAXS profile). The black triangles indicate the expected reflections for a cylindrical morphology ($\sqrt{1}$; $\sqrt{3}$; $\sqrt{4}$; $\sqrt{7}$; $\sqrt{9}$). Corresponding TEM images of the material obtained (left) perpendicularly and (right) parallel to the shear direction (The PS matrix was stained by RuO_4 vapors).

Both 2D patterns obtained perpendicular to the flow direction were anisotropic, and two sets of spots at scattering vectors were separated azimuthally by 180°, as expected for an oriented cylindrical morphology (see Figure S2 in the Supporting Information). The 2D pattern obtained parallel to the direction of the flow exhibited an isotropic ring-like pattern, indicating a lack of long-range hexagonal packing of the oriented cylinders. Transmission electron microscopy (TEM) images, obtained both parallel and perpendicular to the flow direction of the oriented monolith, demonstrated alignment of the cylindrical domains along the shear direction (Figure 2). The diameter of the cylinders was estimated to 19 ± 6 nm from the TEM images, which was in agreement with the value extracted from the SAXS data (23.6 nm).

Sectioning Procedure. Ultramicrotoming is routinely employed for preparing ultrathin sections of materials that can be subsequently observed by TEM. This instrument is based on precisely controlled advancement of an arm holding the sample synchronized with an oscillatory movement applied to the arm. When the extremity of the arm goes down, the sample is forced on the edge of a knife, producing a thin slice of the material. The arm is then moved toward the knife according to the increment

step defined by the user to produce the next slice. Using this instrument, we directly cut a 2 mm × 2 mm square cross-section of our PS−PLA monolith. Diamond knives are usually designed with a cavity on the top called the boat that can be filled with water until the upper edge of the diamond blade is moistened. During the course of monolith microtoming, the sections are floated on the surface of water, which prevents the sections from sticking to the hydrophobic knife-edge. If this occurs, the samples would crumple and quickly accumulate, a problem that would be particularly detrimental to our procedure, where high throughput with limited operator intervention is desirable (Figure 3c).

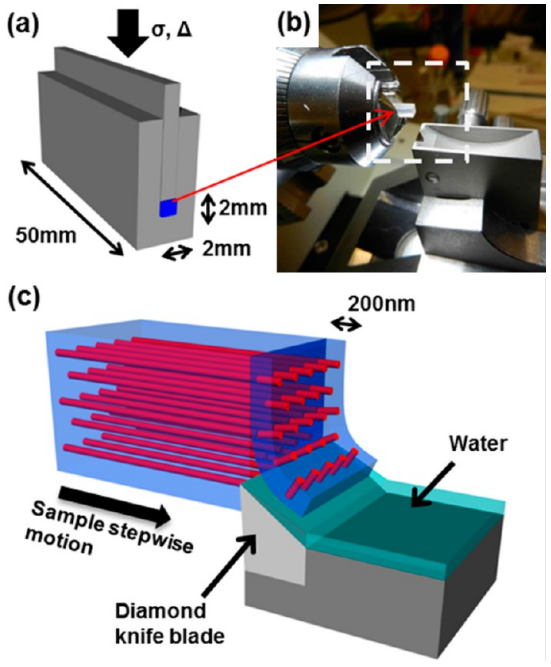

Figure 3. (a) Schematic view of the channel die employed for microstructural alignment (b) Close up photograph of the PS−PLA monolith mounted on the microtome arm that is about to be cut by the diamond knife. (c) Schematic view of the sectioning procedure, the cut slices are floated on the water boat.

When the desired number of sections was reached, the diamond knife is removed, and the water reservoir is emptied into a polypropylene tube, and the water was removed by freeze-drying.

The ability to cut ultrathin sections is largely affected by the mechanical properties of the material. If the material is too soft, it will tend to be deformed, resulting in thickness variations and missed cuts. This undesired behavior can be circumvented by decreasing the operating temperature with liquid nitrogen (cryomicrotomy). However, the water boat is important for our procedure, as it helps to maintain the edge of the knife clean, implying that the cutting process must be done at room temperature. With both PS and PLA blocks being glassy and stiff at room temperature ($T_{g(PS)}$= 100 °C,[21] $T_{g(PLA)}$ = 55 °C[22]), PS−PLA block copolymers are good candidates for this purpose. We employed a 45° diamond knife with a clearance angle of 6° and a width of 3 mm. The cutting speed was typically set at 4 mm/s, producing about 25 sections/min. Each section was expected to contain about 2.4×10^9 individual cylinders, based on the monolith dimensions and the domain spacing extracted from the SAXS analysis of the PS−PLA copolymer. The theoretical particle production rate was estimated to 6×10^{10} particles/min (see the Supporting Information for details). A binocular optical microscope allowed observation of the sections produced. Within each floating section, it appeared that some wrinkling occurred along with stripes of various thicknesses. The combined effects of the large sample width (~2 mm) and the knife likely produced such compression-induced defects.

The dried sections were subsequently dispersed in cyclohexane, a selective solvent for the PS matrix. Particle sizes were estimated by dynamic light scattering (DLS). DLS experiments revealed a monomodal size distribution and a mean hydrodynamic diameter (D_h) of 75 ± 3 nm when the theoretical thickness of the cut slices was 200 nm. As DLS measurements give only an average hydrodynamic size of the particles, TEM imaging was employed to visualize the cylinders in the dry state. TEM samples were prepared by drop-casting from the dilute cyclohexane solution onto copper grids with a Formvar supportive layer. The grids were subsequently exposed to RuO_4 vapors, which selectively stains the PS shell (appears darker on the images, Figure 4).

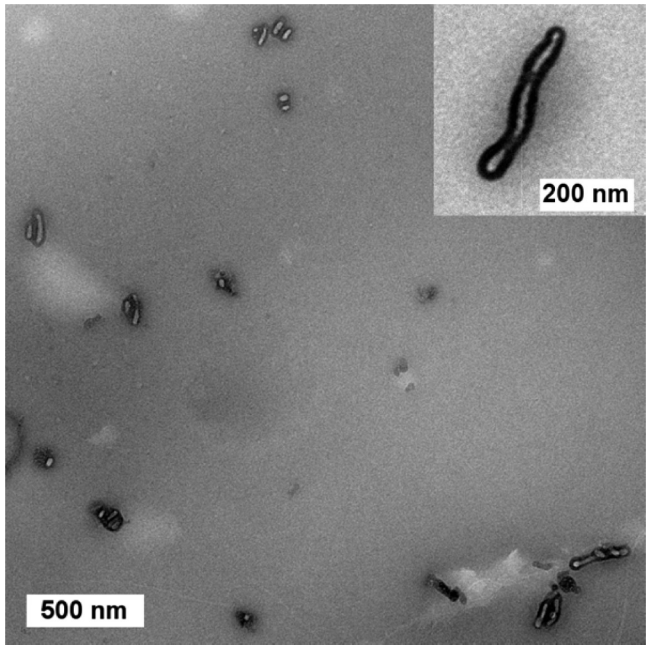

Figure 4. TEM image of PS−PLA nanoparticles casted from a cyclohexane solution (0.02 g L^{-1}) for 200 nm-thick sections. The particles were stained with RuO_4. The TEM sample was prepared by absorbing the excess of solution with a piece of cleaning paper placed under the grid. Inset: A higher-magnification view of an isolated cylindrical nanoparticle revealing its core−shell structure.

Isolated particles along with small aggregates were observed throughout the grid, and the core−shell structures of the nanoparticles were noticeable. Although the diameter of the PLA core (~18−20 nm) was consistent with the cylinder diameter measured for the monolith (19 ± 6 nm by TEM, 23.6 nm by SAXS), the length distribution was somewhat broad, ranging from ~30 to 400 nm. The thickness variations observed during the cutting process could be the main reason for this result. In addition, the quality of the alignment can also affect the size distribution of the particles; first, if the cylinders are not completely parallel to the shear flow (perpendicular to the edge of knife), they will result in nanocylinders with longer lengths and consequently particles with greater average size. Second, smaller particles will be produced if the cylinders are not contiguous throughout the sample.

As the PS−PLA copolymer showed promising results for nanocylinder fabrication via block copolymer self-assembly and nanoskiving, we also explored extension of our procedure for water-dispersible nanoparticles. To generate hydrophobic particle cores with water-soluble coronae a poly(*N*,*N*-dimethylacrylamide)-*b*-poly(styrene) (PDMA−PS) block copolymer was synthesized using reversible addition−fragmentation chain transfer (RAFT) controlled radical polymerization, with S-dodecyl-S′-(isobutyric acid) trithiocarbonate (DIBTTC) as the chain transfer agent (CTA) and α,α'-azobis(isobutyronitrile) (AIBN) as the initiator (Scheme 1).[23] Block molar masses for the copolymer used in this study, determined by NMR spectroscopy, were 25 kg/mol and 12 kg/mol for the PDMA and PS blocks, respectively, which corresponds to 36 volume percent of PS. The composition was tuned for cylindrical morphology, and this copolymer was expected to form hydrophobic PS cylinders into a water-soluble PDMA matrix.

Scheme 1. Synthetic Pathway for the Synthesis of PDMA−PS Block Copolymer by RAFT Polymerization

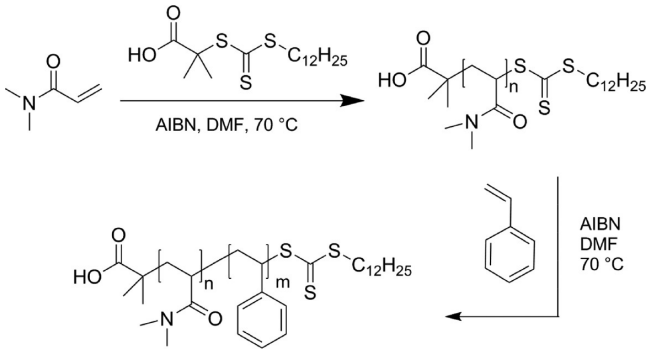

The copolymer was processed at 160 °C in the same home-built channel die employed for the PS−PLA samples, and the microstructure of the resulting monolith was investigated by SAXS and TEM (sample A). To illustrate the consistency and reproducibility of our method, characterization details of second sample prepared using the same conditions is provided in the Supporting Information (referred to as sample B). SAXS analysis of the resulting monolith revealed an intense primary peak at $q^* = 0.197$ nm ($D^* = 31.9$ nm^{-1}) along with numerous higher order reflections at $\sqrt{4}q^*$, $\sqrt{7}q^*$, $\sqrt{9}q^*$, $\sqrt{12}q^*$, $\sqrt{13}q^*$, and $\sqrt{16}q^*$, unambiguously indicative of a cylindrical morphology (Figure 5, and Figure S7 in the Supporting Information for Sample B). Similar to the PS−PLA monolith, the 2D SAXS patterns obtained parallel to the shear direction are anisotropic, hence demonstrating the microstructural alignment (see Figure S6 in the Supporting Information). In agreement with SAXS results, TEM images showed a well-aligned specimen. In particular, hexagonally packed cylinders were evident when imaging in the shear flow direction. The cylinder diameter was estimated to be 19 ± 5 nm, in agreement with the value extracted from the SAXS data (22.6 nm).

Since both PDMA and PS are also glassy at room temperature ($T_{g(PDMA)} = 112$ °C,[24] $T_{g(PS)} = 100$ °C[21]), the monolith was sectioned at room temperature. For the PDMA−PS copolymer, however, the water boat used to float the cut slices is also a selective solvent for the PDMA matrix, and this can potentially eliminate the need for freeze-drying as the dispersions can be formed in the water reservoir on the diamond knife upon sectioning. However, to prepare solutions with a known concentration, the resulting dispersions were freeze-dried, and the sample was diluted with water for DLS and TEM analyses. From the monolith dimensions, 2 mm × 2 mm, and the domain spacing extracted from the SAXS analysis, each section is expected to contain about 3.6×10^9 cylinders (9×10^{10} particles/min with 25 sections/min). Once a cut slice was introduced to the water boat, it did not immediately dissolve and appeared to be a highly swollen sheet floating on the water. Thus, to be certain that the cylinders were well dispersed in the solvent, the solutions were shaken for about 30 min after they were transferred into a plastic centrifuge tube.

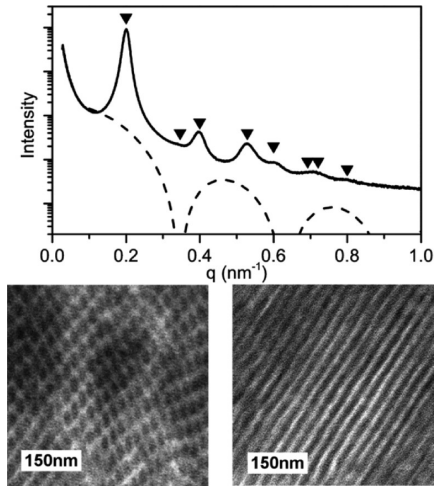

Figure 5. (Solid line) Experimental 1D synchrotron SAXS profile of shear-oriented PDMA−PS monolith (sample A) at 25 °C and (dashed line) simulated form factor scattering curve generated for cylinders with an 11.3 nm radius (value extracted from the experimental SAXS profile). The black triangles indicate the expected reflections for a cylindrical morphology ($\sqrt{1}$; $\sqrt{3}$; $\sqrt{4}$; $\sqrt{7}$; $\sqrt{9}$; $\sqrt{12}$; $\sqrt{13}$; $\sqrt{16}$). Corresponding TEM images of the material, obtained (left) perpendicularly and (right) parallel to the shear direction (PS domains, appearing darker, were stained by RuO_4 vapors).

Prior to TEM characterization of the samples, the carbon/Formvar-coated TEM grids were treated with air plasma (glow discharge) to improve their hydrophilicity. Two different sample preparation methods were used: (i) droplets of the solution were placed on the grid and the solvent was allowed to evaporate, and (ii) a piece of cleaning paper was placed under the grid to absorb the solvent. Figure 6 and Figure S10 in the Supporting Information compare images acquired with these two different methods; these images were taken before sonication of the samples. As evident from the images, in the latter method (ii), because of the quick absorption of the solvent and removing most of the particles by the paper placed underneath, no accumulation of cylinders was observed. Whereas, in the former method (i), all of the particles dry on the grid and slow evaporation of the solvent allows the particles to aggregate. From the images (Figure 6b, c), the average length of the cylinders is estimated to be about 480 nm with ∼10% variation. Although the size distribution seems to be off the targeted length of 200 nm, there is a reasonable control on the length of the cylinders. To produce longer cylinders, 300 nm thick sections were also prepared. Similar to the aforementioned results, we observed by TEM cylinders relatively homogeneous in size, with an average length of approximately 600 nm (see Figure S12 in the Supporting Information). It is certainly possible to achieve fiberlike particles by increasing the thickness. However, targeting

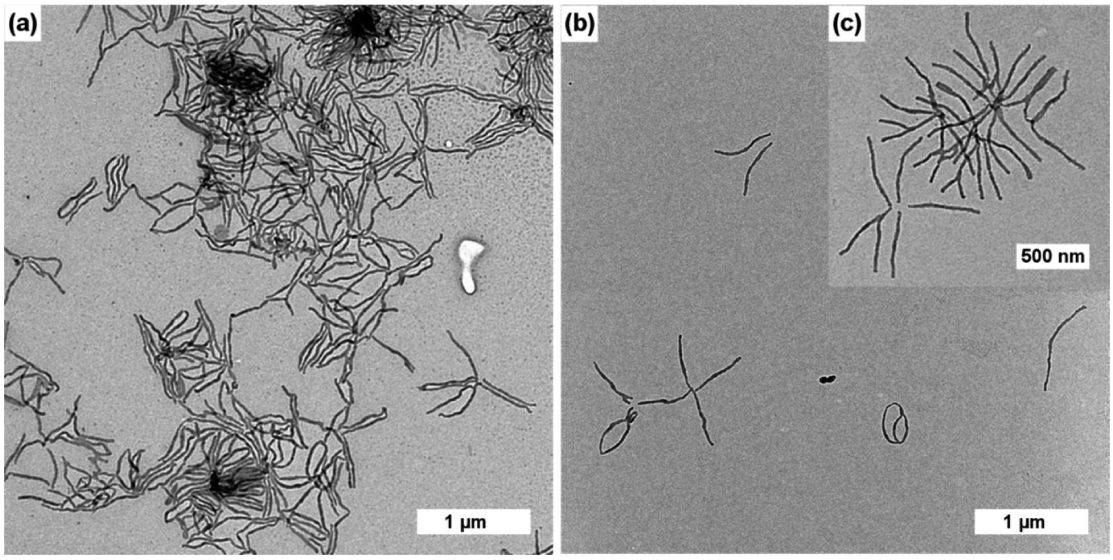

Figure 6. (a) TEM image of PS−PDMA nanoparticles (sample A) casted from an aqueous solution (0.2 g L^{-1}). The carbon/Formvar-coated TEM grids were treated with air plasma to improve their hydrophilicity prior to use. The nanoparticles were stained with RuO_4. (a) Sample prepared through complete evaporation of the water in a droplet placed on the grid (method i). (b, c) Sample prepared by absorbing the excess of solution with a piece of paper placed under the grid (method ii).

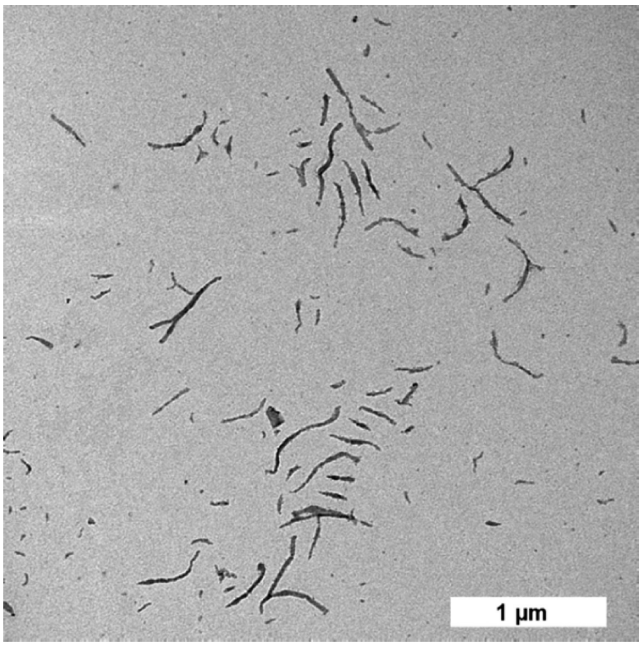

Figure 7. TEM image of PS−PDMA nanoparticles (sample A) casted from an aqueous solution (0.2 g L^{-1}) after 5 min of sonication. The carbon/Formvar-coated TEM grids were treated with air plasma to improve their hydrophilicity prior to use. The nanoparticles were stained with RuO_4. The sample was prepared by absorbing the excess of solution with a piece of paper placed under the grid (method ii).

bigger particles might result in a higher proportion of defected structures.

In both cases, some nanocylinders seem to be aggregated at their ends, a possible indication of sample damage during the cutting step. To break any nondispersed materials, the dispersions were sonicated for 3 to 5 min. Although sonication seems to be efficient in breaking aggregates, it results in appearance of smaller particles in a broader size range, implying that some of the cylinders are broken/damaged upon sonication (Figures 7, and Figure S11 in the Supporting Information for Sample B). The average length of the cylinders was estimated to 290 ± 150 nm after sonication. The major variation observed in the size distribution of more than 50% is likely due to the breakage of the cylinders, an issue that could possibly be circumvented by optimizing the sonication conditions. According to DLS, the average size of the cylinders decreases from 189 ± 9 nm to 163 ± 8 nm with sonication (see Figures S8 and S9 in the Supporting Information).

CONCLUSION

Herein, an approach for nanoparticle fabrication that combines block copolymer self-assembly and nanoskiving is introduced. This fabrication method allows a facile experimental procedure that does not require specialty fabrication equipment. While maintaining many advantages of the other top-down approaches, e.g., specific shape fidelity, and some degree of control on the size, our new approach utilizes block copolymer self-assembly to form the nanostructures in their thermodynamically stable state. This is advantageous because it is expected to result in nanoparticles with homogeneous and optimized surfaces, the mechanical altering on the nanoparticles surface is minimized, and only the ends of the cylinders are formed in a nonoptimal condition due to the cutting step. The production of particles that are surrounded by a stabilizing corona is another advantage of this approach to nanoparticle fabrication. Simple synthesis procedures and easy accessibility to cylindrical nanostructures in a range of compositions (~25−35%) through controlled polymerizations allow a versatile choice of materials for nanoparticle fabrications using this technique. Successfully illustrated with a PS−PLA and a PDMA−PS diblock copolymer, we expect this fabrication method to be usable with any glassy self-assembled block copolymer sample.

ASSOCIATED CONTENT

Supporting Information

Experimental procedures, Figures S1−S11, and Table S1. This material is available free of charge via the Internet at http://pubs.acs.org.

AUTHOR INFORMATION

Corresponding Authors

*E-mail: hillmyer@umn.edu.
*E-mail: treineke@umn.edu.

Author Contributions

†M.N. and A.B. contributed equally to this work.

Notes

The authors declare no competing financial interest.

ACKNOWLEDGMENTS

This work was supported by the National Institutes of Health Director's New Innovator Award Program (DP2OD006669-01) and the National Science Foundation (DMR-1006370). We thank Dr. Justin Bolton for the synthesis of the RAFT agent and Dr. Marc Rodwogin and Dr. Elizabeth Jackson for the synthesis of the PS−PLA copolymer. Parts of this work were carried out in the Characterization Facility, University of Minnesota, which receives partial support from NSF through the MRSEC and NNIN programs. Synchrotron SAXS data were obtained at the DuPont-Northwestern-Dow Collaborative Access Team (DND-CAT) located at Sector 5 of the Advanced Photon Source (APS). DND-CAT is supported by E.I. DuPont de Nemours & Co., The Dow Chemical Company, and Northwestern University. Use of the APS at Argonne national Laboratory was supported by the U.S. Department of Energy, Office of Science, Office of Basic Energy Sciences, under Contract DE-AC02-06CH11357.

REFERENCES

(1) Euliss, L. E.; DuPont, J. A.; Gratton, S.; DeSimone, J. M. Imparting Size, Shape, and Composition Control of Materials for Nanomedicine. *Chem. Soc. Rev.* **2006**, *35*, 1095−1104.

(2) Biswas, A.; Bayer, I. S.; Biris, A. S.; Wang, T.; Dervishi, E.; Faupel, F. Advances in top-down and bottom-up surface nanofabrication: Techniques, Applications & Future Prospects. *Adv. Colloid Interface Sci.* **2012**, *170*, 2−27.

(3) Devadasu, V. R.; Bhardwaj, V.; Kumar, M. N. V. R. Can Controversial Nanotechnology Promise Drug Delivery? *Chem. Rev.* **2013**, *113*, 1686−1735.

(4) Zhang, L. F.; Eisenberg, A. Multiple Morphologies of Crew-cut Aggregates of Polystyrene-b-poly(acrylic acid) Block-copolymers. *Science* **1995**, *268*, 1728−1731.

(5) Hu, J.; Njikang, G.; Liu, G. Twisted ABC Triblock Copolymer Cylinders with Segregated A and C Coronal Chains. *Macromolecules* **2008**, *41*, 7993−7999.

(6) Li, X.; Liu, G.; Han, D. Wrapping Amino-bearing Block Copolymer Cylinders Around Carboxyl-bearing Nanofibers: A Case of Hierarchical Assembly. *Soft Matter* **2011**, *7*, 8216−8223.

(7) Choi, S.-H.; Bates, F. S.; Lodge, T. P. Molecular Exchange in Ordered Diblock Copolymer Micelles. *Macromolecules* **2011**, *44*, 3594−3604.

(8) Lund, R.; Willner, L.; Richter, D. In *Controlled Polymerization and Polymeric Structures*; Abe, A., Lee, K.-S., Leibler, L., Kobayashi, S., Eds.; Springer International Publishing: 2013; Vol. *259*, pp 51−158.

(9) Badaire, S.; Cottin-Bizonne, C.; Woody, J. W.; Yang, A.; Stroock, A. D. Shape Selectivity in the Assembly of Lithographically Designed Colloidal Particles. *J. Am. Chem. Soc.* **2007**, *129*, 40−41.

(10) Merkel, T. J.; Herlihy, K. P.; Nunes, J.; Orgel, R. M.; Rolland, J. P.; DeSimone, J. M. Scalable, Shape-Specific, Top-Down Fabrication Methods for the Synthesis of Engineered Colloidal Particles. *Langmuir* **2010**, *26*, 13086−13096.

(11) Canelas, D. A.; Herlihy, K. P.; DeSimone, J. M. Top-down Particle Fabrication: Control of Size and Shape for Diagnostic Imaging and Drug Delivery. *Wiley Interdiscip. Rev. Nanomed. Nanobiotechnol.* **2009**, *1*, 391−404.

(12) Varadan, V. K.; Chen, L.; Xie, J. *Nanomedicine: Design and Applications of Magnetic Nanomaterials, Nanosensors and Nanosystems*; John Wiley & Sons: Chichester, UK, 2008.

(13) Kim, H.-C.; Park, S.-M.; Hinsberg, W. D. Block Copolymer Based Nanostructures: Materials, Processes, and Applications to Electronics. *Chem. Rev.* **2010**, *110*, 146−177.

(14) Zalusky, A. S.; Olayo-Valles, R.; Wolf, J. H.; Hillmyer, M. A. Ordered Nanoporous Polymers from Polystyrene-Polylactide Block Copolymers. *J. Am. Chem. Soc.* **2002**, *124*, 12761−12773.

(15) Drzal, P. L.; Barnes, J. D.; Kofinas, P. Path Dependent Microstructure Orientation During Strain Compression of Semicrystalline Block Copolymers. *Polymer* **2001**, *42*, 5633−5642.

(16) Rzayev, J.; Hillmyer, M. A. Nanochannel Array Plastics with Tailored Surface Chemistry. *J. Am. Chem. Soc.* **2005**, *127*, 13373−13379.

(17) Bertrand, A.; Hillmyer, M. A. Nanoporous Poly(lactide) by Olefin Metathesis Degradation. *J. Am. Chem. Soc.* **2013**, *135*, 10918−10921.

(18) Xu, Q. B.; Gates, B. D.; Whitesides, G. M. Fabrication of Metal Structures with Nanometer-Scale Lateral Dimensions by Sectioning Using a Microtome. *J. Am. Chem. Soc.* **2004**, *126*, 1332−1333.

(19) Xu, Q.; Rioux, R. M.; Dickey, M. D.; Whitesides, G. M. Nanoskiving: A New Method To Produce Arrays of Nanostructures. *Acc. Chem. Res.* **2008**, *41*, 1566−1577.

(20) Lipomi, D. J.; Martinez, R. V.; Whitesides, G. M. Use of Thin Sectioning (Nanoskiving) to Fabricate Nanostructures for Electronic and Optical Applications. *Angew. Chem., Int. Ed.* **2011**, *50*, 8566−8583.

(21) Shen, M. C.; Eisenberg, A. Glass Transitions in Polymers. *Rubber Chem. Technol.* **1970**, *43*, 95−155.

(22) Hyon, S. H.; Jamshidi, K.; Ikada, Y. Effects of Residual Monomer on the Degradation of DL-Lactide Polymer. *Polym. Int.* **1998**, *46*, 196−202.

(23) Faber, M.; Hofman, A. H.; Polushkin, E.; van Ekenstein, G. A.; Seitsonen, J.; Ruokolainen, J.; Loos, K.; ten Brinke, G. Hierarchical Self-Assembly in Supramolecular Double-Comb Diblock Copolymer Complexes. *Macromolecules* **2013**, *46*, 500−517.

(24) Chiantore, O.; Costa, L.; Guaita, M. Glass Temperatures of Acrylamide Polymers. *Makromol. Chem. Rapid Commun.* **1982**, *3*, 303−309.